© 2016. Published by The Company of Biologists Ltd | Journal of Cell Science (2016) 129, 2778-2792 doi:10.1242/jcs.182824

RESEARCH ARTICLE

Endosomal assembly and transport of heteromeric septin complexes promote septin cytoskeleton formation

Sabrina Zander[1,‡], Sebastian Baumann[1,*,‡], Stefanie Weidtkamp-Peters[2] and Michael Feldbrügge[1,§]

ABSTRACT

Septins are conserved cytoskeletal structures functioning in a variety of biological processes including cytokinesis and cell polarity. A wealth of information exists on the heterooligomeric architecture of septins and their subcellular localization at distinct sites. However, the precise mechanisms of their subcellular assembly and their intracellular transport are unknown. Here, we demonstrate that endosomal transport of septins along microtubules is crucial for formation of higher-order structures in the fungus *Ustilago maydis*. Importantly, endosomal septin transport is dependent on each individual septin providing strong evidence that septin heteromeric complexes are assembled on endosomes. Furthermore, endosomal trafficking of all four septin mRNAs is required for endosomal localization of their translation products. Based on these results, we propose that local translation promotes the assembly of newly synthesized septins in heteromeric structures on the surface of endosomes. This is important for the long-distance transport of septins and the efficient formation of the septin cytoskeleton.

KEY WORDS: Early endosomes, mRNA transport, Septin, RNA recognition motif

INTRODUCTION

Septins are GTP-binding cytoskeletal proteins that are evolutionarily highly conserved from fungi to mammals (Beise and Trimble, 2011; Fung et al., 2014). They are involved in diverse processes, such as cell division, neuronal development or plant invasion by fungal pathogens (Bridges and Gladfelter, 2014, 2015). In humans dysfunctions of septins have been implicated in cancer and neurodegenerative diseases (Bridges and Gladfelter, 2015; Dolat et al., 2013).

A characteristic feature of septins is the central GTP-binding domain that is flanked by a polybasic region involved in membrane binding at the N-terminus (Bridges and Gladfelter, 2015). Most commonly a palindromic nonpolar heterooctamer is formed by four different septins. In *Saccharomyces cerevisiae*, for example, the septins Cdc3, Cdc10, Cdc11 and Cdc12 form the defined hetero-octamer Cdc11–Cdc12–Cdc3–Cdc10–Cdc10–Cdc3–Cdc12–Cdc11. Interactions between, for example, Cdc12–Cdc3, Cdc10–Cdc10 and Cdc11–Cdc11 at the so-called 'NC' interface are essential (Beise and Trimble, 2011; Sirajuddin et al., 2007). The terminal subunit Cdc11 can be replaced by an alternative septin subunit Shs1, resulting in the formation of alternative heterooctamers (Booth et al., 2015; Finnigan et al., 2015; Garcia et al., 2011).

Such heterooctameric building blocks can anneal head to tail into longer rods, which are bundled at specific subcellular locations to form higher-order structures, such as rings or filaments. Such structures are found for example at the division site between mother and daughter cells in *S. cerevisiae* (Bridges et al., 2014) or at the base of dendritic spines in neurons (Tada et al., 2007; Xie et al., 2007). Extended filamentous structures are mainly known from mammalian cells, where they partly colocalize with F-actin and distinct subsets of modified microtubules (Spiliotis and Gladfelter, 2012; Spiliotis et al., 2008). Even though the structure of septin heterooligomers has been analysed in great detail, it is still unclear precisely how septins are assembled and how they reach their subcellular destination (Bridges and Gladfelter, 2015).

We are studying septin biology in *Ustilago maydis*, a fungal pathogen causing corn smut disease. Its genome encodes the core septins Cdc3, Cdc10, Cdc11 and Cdc12 (UMAG_10503, UMAG_10644, UMAG_03449 and UMAG_03599, respectively). However, a clear Shs1 orthologue is missing (Alvarez-Tabares and Perez-Martin, 2010; Böhmer et al., 2009). A prerequisite for infection is the switch from yeast to hyphal growth (Vollmeister et al., 2012). Hyphae grow with a defined axis of polarity expanding at the apical tip and inserting septa at the basal pole (Vollmeister and Feldbrügge, 2010). An essential process involved in polar growth is long distance transport of macromolecules such as proteins, lipids as well as mRNAs (Haag et al., 2015; Jansen et al., 2014). Rab5a-positive endosomes act as important carriers that shuttle along microtubules mediated by the plus-end directed motor Kin3 and the minus-end directed motor dynein (Lenz et al., 2006; Schuster et al., 2011; Steinberg, 2014).

The key factor for mRNA transport is the RNA-binding protein Rrm4, which contains three RNA recognition motifs (RRM) at the N-terminus and two peptide-binding MLLE-domains (Becht et al., 2005; Pohlmann et al., 2015). The MLLE domains interact with Upa1, an endosomal component that functions in recruiting Rrm4 to Rab5a-positive endosomes (Pohlmann et al., 2015). The RRMs bind target mRNAs encoding, for example, the septin Cdc3 (König et al., 2009). Characterization of the transport of *cdc3* mRNA led to the model that local translation of *cdc3* mRNA mediates loading of Cdc3 protein onto the cytoplasmic surface of endosomes for microtubule-dependent transport. This process is crucial for efficient formation of a septin gradient in cortical filaments at the hyphal growth pole (Baumann et al., 2014; Jansen et al., 2014). A second septin, Cdc12, also shuttles in a microtubule-dependent manner on endosomes, raising the possibility that septin heterooligomers might assemble on endosomes for subcellular transport (Baumann et al., 2014). Here, we provide detailed *in vivo* evidence that all septins are indeed transported on endosomes in an interdependent manner to support the

[1]Department of Biology, Institute for Microbiology, Cluster of Excellence on Plant Sciences, Heinrich Heine University Düsseldorf, 40204 Düsseldorf, Germany.
[2]Department of Biology, Center for Advanced Imaging (CAi), Heinrich Heine University Düsseldorf, 40204 Düsseldorf, Germany.
*Present address: Cell and Developmental Biology, Centre for Genomic Regulation (CRG), Barcelona, Spain.
‡These authors contributed equally to this work

§Author for correspondence (feldbrue@hhu.de)

M.F., 0000-0003-0046-983X

Received 30 October 2015; Accepted 26 May 2016

Journal of Cell Science

Journal of Cell Science (2016) 129, 2778-2792 doi:10.1242/jcs.182824

formation of higher-order structures at the growth pole. This suggests that preassembly of septin heterooligomers takes place on the membranous surface of endosomes.

RESULTS

Septins are important for polar growth and unconventional secretion

Cdc3 is needed for efficient hyphal growth of *U. maydis* (Baumann et al., 2014). To address whether the other three septins perform similar functions we generated deletion mutants in the genetic background of strain AB33 (Tables S1, S2). In this strain, formation of hyphae can be elicited by switching the nitrogen source (Brachmann et al., 2001). Wild-type hyphae show mainly unipolar growth, expanding at the apical pole while inserting septa at the basal pole (Fig. 1A). All four septin deletion strains developed a substantial number of hyphae showing bipolar growth at 4 h post induction (h.p.i.; Fig. 1A,B). This resembles the growth defects observed in *rrm4Δ* strains (Becht et al., 2006). At later stages a large proportion of hyphae of septin deletion strains recovered and switched to unipolar growth with basal septa (8 h.p.i.; Fig. 1A,B). However, compared to wild-type, septin deletion strains contained an increased amount of bipolar hyphae without septa (8 h.p.i.) indicating that these mutations cause defects in establishing unipolar hyphal growth (Fig. 1B).

As a second read-out we tested unconventional secretion of chitinase Cts1 (Stock et al., 2012), a process that is specifically dependent on Rrm4-mediated mRNA transport during hyphal growth (Koepke et al., 2011). We observed that all four septin deletion strains exhibited reduced secretion of Cts1 only in hyphae (Fig. 1C). Thus, all four septins are needed for efficient unipolar growth and unconventional secretion of Cts1 indicating a common function for septins during hyphal growth.

All septins localize to shuttling endosomes and in filaments

Fluorescently tagged fusion proteins are best suited to study *in vivo* septin biology. Therefore, we generated a comprehensive collection of strains in the genetic background of AB33, expressing septins fused N- or C-terminally to the green fluorescent protein (eGfp, Clontech) at the endogenous locus. Notably, the 3′ untranslated region (UTR) was preserved to keep potential regulatory elements intact (Fig. S1A).

We tested the functionality of the fusion proteins in a growth assay for bipolar filaments and in the Cts1 secretion assay (Fig. S1B,C). Two main observations were made in these experiments. First, a functional Cdc3 wild-type protein was most closely resembled by the N-terminal fusion of Cdc3 (Cdc3–GfpN) whereas the corresponding C-terminal fusion was less functional. Second, the remaining fusion proteins of the other septins complemented the deletion phenotype to various extents.

Visualizing the subcellular localization of all septin fusion proteins revealed that they accumulated at basal septa and in cytoplasmic rings (Fig. 2A,B; Fig. S2A). The latter might either serve as transient storage forms or could be indicative of assembly defects (Böhmer et al., 2009). Certain fusion proteins tend to form these rings more often than others (Fig. S2B). Importantly, all fusion proteins localized to shuttling units that moved with a comparable speed of about 2.3 µm/s in both directions throughout the whole hypha (Fig. 2C–E; Movies 1–4). In all cases, the movement was affected by the microtubule inhibitor benomyl (Fig. 2D; Movie 5). Benomyl prevents polymerization of microtubules and therefore long-distance transport along microtubules is abolished. This results in the formation of bipolarly growing hyphae (Fuchs et al., 2005; Higuchi et al., 2014) resembling those from *rrm4Δ* hyphae (Fig. 1A; Becht et al., 2006). To identify the shuttling units, we briefly stained hyphae with the lipophilic dye FM4-64. This dye follows the endocytotic pathway (Vida and Emr, 1995) and is widely used to stain Rab5a-positive early endosomes in *U. maydis* (Higuchi et al., 2014). We observed that all septins colocalized with FM4-64 positive units. Thus, as shown for Cdc3 (Baumann et al., 2014), all septins are present on shuttling endosomes (Fig. S2C).

Finally, we studied filament formation of all septin fusion proteins (Fig. 2F). For clear visualization of cortical filaments, we analysed maximum intensity projections of *z*-planes (Baumann et al., 2014). We observed that all septins were present in cortical filaments running along the longitudinal axis of hyphae (Fig. 2F). However, depending on the position of the fused Gfp, the filaments differed in their appearance (see Discussion). For example, Cdc3–GfpN formed filaments with a gradient emanating from the hyphal tip, whereas Cdc3–GfpC formed only very short, aberrant filaments (Fig. 2F; Fig. S2D). The cortical filaments in Cdc10–GfpN exhibited a different appearance in that they did not reach the hyphal tip and only a slight gradient was observed (Fig. 2F, Fig. S2D). Filament formation itself was not inhibited by benomyl, but in this case the gradient was also lost (compare Fig. 2F and Fig. S2E), suggesting that microtubule-dependent transport is needed for gradient formation (Baumann et al., 2014). Some fusions (e.g. Cdc3–GfpC or Cdc12–GfpC) failed to form extended filaments, suggesting that the Gfp fusion site interferes with the formation of higher-order structures. In summary, consistent with results obtained analysing Cdc3 (Baumann et al., 2014), all other septins also localize to endosomes shuttling on microtubules as well as to cortical filaments.

Septins colocalize at distinct subcellular sites and Cdc3 interacts with Cdc12 directly

To verify that septin proteins colocalize at the distinct subcellular sites described above, we studied colocalization of two neighbouring septin pairs, Cdc3–CherryN (N-terminal fusion with mCherry) with either Cdc10–GfpC or Cdc12–GfpN. Expression of the mCherry fusion protein was driven by the strong promoter P_{otef} to improve detection of the mCherry signal (Shaner et al., 2004). As expected, for both septin pairs, the proteins colocalized at septa and in cytoplasmic rings (Fig. 3A). Moreover, using dual-view technology, extensive colocalization on shuttling endosomes was detected (Fig. 3B,C; Movies 6,7).

Furthermore, single-plane analysis revealed wide-ranging colocalization of both septins in cortical filaments (Fig. 3D). Interestingly, the gradient of Cdc3–CherryN was no longer observed in a strain co-expressing Cdc12–GfpN (Fig. S3A, lower left panel). This suggests that the presence of Cdc12–GfpN alters the filament-forming ability of Cdc3–CherryN (compared to a strain expressing only Cdc3-CherryN; Fig. S3A, upper left panel), suggesting a direct Cdc3–Cdc12 interaction in these septin filaments.

To verify the interaction, we performed basic fluorescence resonance energy transfer (FRET) and more rigorous fluorescence lifetime imaging microscopy (FLIM)-FRET experiments. Analysing hyphal tips revealed that bleaching the mCherry acceptor of Cdc3–CherryN resulted in a clear increase (~6%, Fig. S3B) in Gfp fluorescence of Cdc12–GfpN (donor) in the hyphal tip. In agreement, the Gfp lifetime of Cdc12–GfpN measured in FLIM-FRET experiments was significantly lower in strains co-expressing Cdc3–CherryN in comparison to the control

Journal of Cell Science (2016) 129, 2778-2792 doi:10.1242/jcs.182824

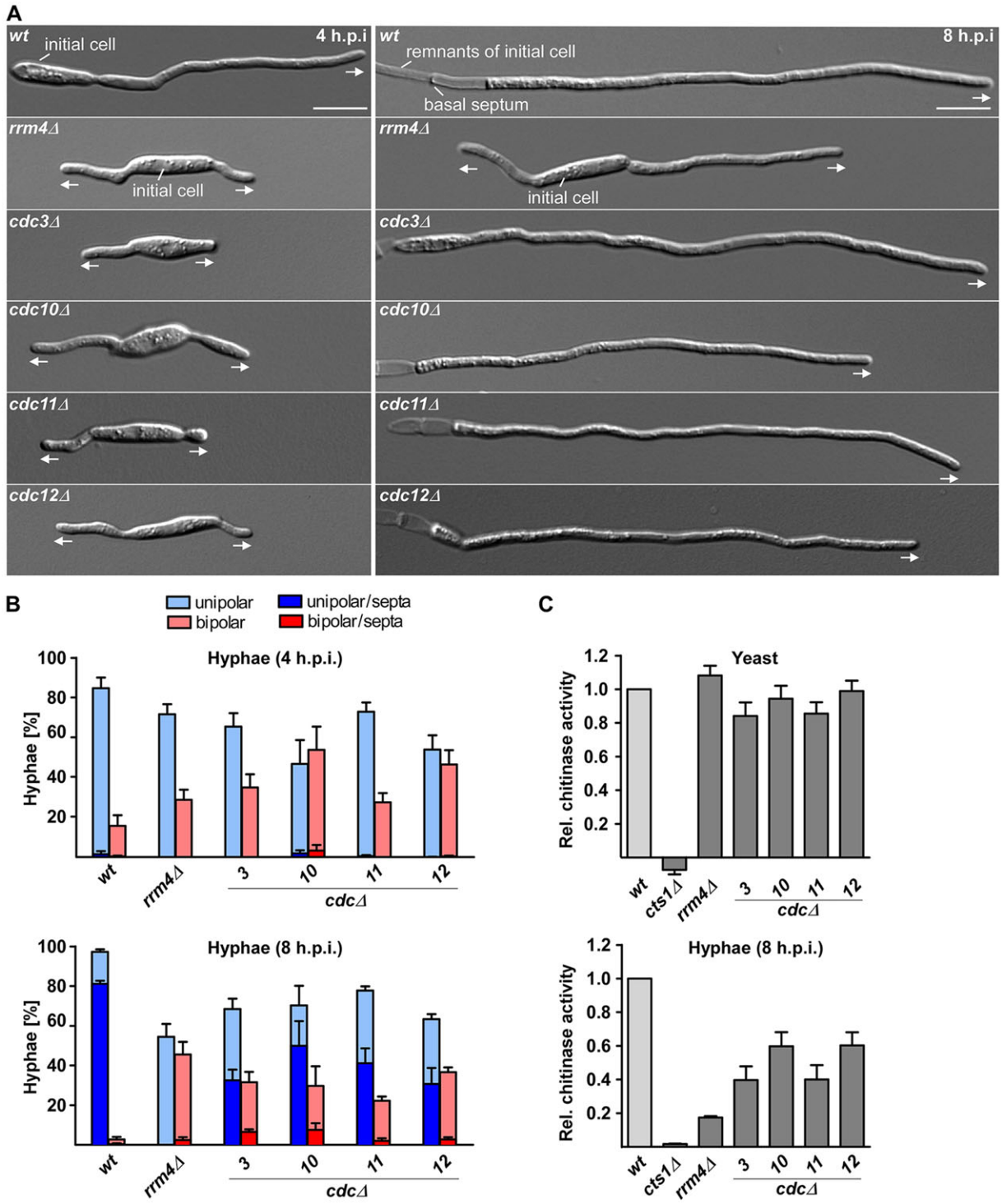

Fig. 1. All four septins are needed for efficient polar growth and endochitinase secretion. (A) Hyphae of AB33 derivatives at 4 h (left) and 8 h (right) after induction of polar growth (DIC images). Growth direction is marked by arrows. Scale bars: 10 µm. (B) Percentages of hyphae after 4 h.p.i. (top) and 8 h.p.i. (bottom): unipolarity, bipolarity and septum formation were quantified (error bars represent mean±s.e.m.; *n*=4 independent experiments, at least 50 hyphae were counted per strain and experiment; note that septum formation is given relative to the values of unipolar or bipolar hyphae set at 100%). (C) Relative chitinase activity of septin deletion strains as assessed by detecting endochitinase Cts1 (Koepke et al., 2011; Langner et al., 2015) in the yeast (top) or hyphal form (bottom; 8 h.p.i.). Error bars represent mean±s.e.m.; *n*=7 independent experiments.

(Fig. 3E, left). Measuring the Gfp lifetime in strains expressing Cdc3–CherryN and Cdc10–GfpC revealed that the lifetime was not significantly altered in comparison to the corresponding control strain (Fig. 3E). Thus, as predicted from structural data from *S. cerevisiae* and humans (Beise and Trimble, 2011; McMurray et al., 2011; Sirajuddin et al., 2007; Versele et al., 2004), the N-termini of Cdc3 and Cdc12 are in close proximity. This is not the case for the N- and C-termini from Cdc3 and Cdc10, respectively. Taken together, septins colocalize at the described subcellular sites, such as shuttling endosomes, and in identical cortical filaments.

Journal of Cell Science (2016) 129, 2778-2792 doi:10.1242/jcs.182824

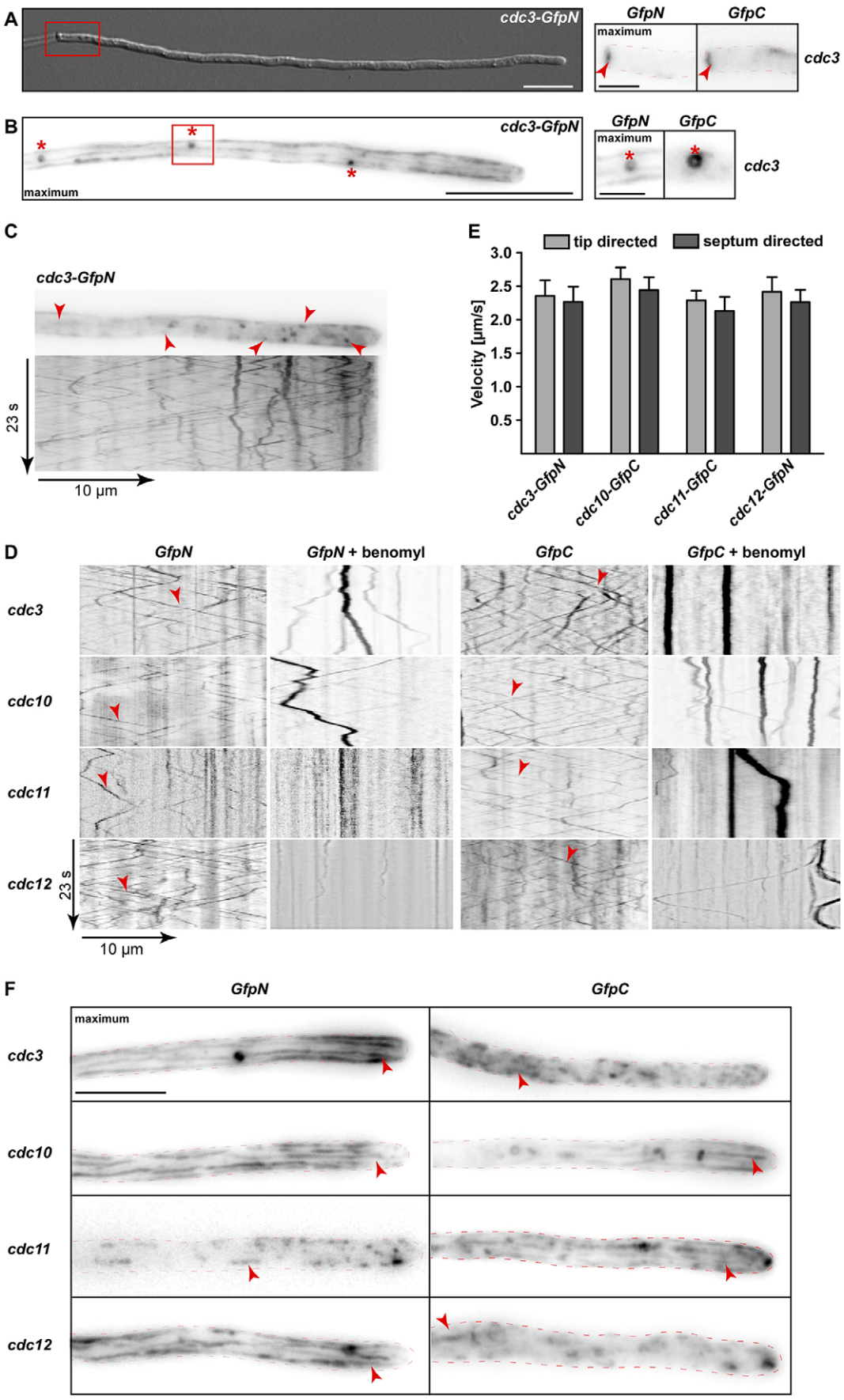

Fig. 2. See next page for legend.

Journal of Cell Science (2016) 129, 2778-2792 doi:10.1242/jcs.182824

Fig. 2. All septins shuttle on endosomes along microtubules and localize in cortical filaments. (A) DIC image of hypha expressing Cdc3–GfpN (left). The red rectangle indicates the septal region enlarged on the right. Fluorescence micrographs of strains expressing Gfp fused either to the N- or C-terminus of Cdc3 (right); septa are indicated by arrowheads (inverted signals, maximum intensity projections). Scale bars: 10 µm (left); 2 µm (right). (B) Fluorescence micrograph of Cdc3–GfpN-expressing strain (left). The red rectangle indicates comparable regions exhibited on the right, asterisks mark cytoplasmic rings. Micrographs of strain expressing Cdc3–GfpN or Cdc3–GfpC (right; inverted signals, maximum intensity projections. Scale bars: 10 µm (left); 2 µm (right). (C) Micrograph of Cdc3–GfpN-expressing hyphae. Shuttling units are indicated by red arrowheads (top). Movement of the units over time is visualized by a kymograph (bottom). (D) Kymographs of strains expressing Gfp fused to Cdc3, Cdc10, Cdc11 and Cdc12 in hypha (see Fig. S1; Movies 1–4). N-terminal Gfp fusion proteins are shown on the left and C- terminal Gfp fusion proteins are shown on the right with their corresponding kymographs of hyphae treated with microtubule inhibitor benomyl (Movie 5). Red arrowheads indicate examples of moving units. (E) Bar diagram showing the velocity of Cdc3–GfpN, Cdc10–GfpC, Cdc11–GfpC and Cdc12–GfpN particles (at least 10 hyphae were counted per strain; error bars represent mean±s.d.). (F) Micrographs of hyphal tips expressing Gfp fused to the N- or C-terminus (left and right, respectively) of septins (indicated to the left; maximum intensity projections). Red arrowheads indicate examples of septin filaments. Scale bar: 5 µm.

This clarifies contradicting results in the literature on septin filaments in filamentous fungi (see Discussion).

Heteromeric septin units are present on shuttling endosomes and in filaments

To address whether septins form heteromeric structures on endosomes, we chose a genetic approach to study the subcellular localization of each septin in the absence of the others. Initially, we verified that deletion of septins did not alter the amount or the processive movement of FM4-64-stained endosomes. In contrast, loss of kinesin-3 type Kin3 resulted in strongly reduced shuttling endosomes (Fig. S3C). Thus, endosomal septins are dispensable for the motility of endosomes.

Next, we concentrated on one Gfp fusion for each septin (Fig. S1) to analyse the interdependency of their subcellular localization. Importantly, absence of one septin caused either a severe reduction or complete loss of endosomal localization of the other septins (Fig. 4A). Cdc3–GfpN localization, for example, was greatly reduced on endosomes in the absence of Cdc10 or Cdc11 and undetectable in the absence of Cdc12 (Fig. 4A). This suggests that heteromeric septin assemblies are formed on endosomes. In case of Cdc12–GfpN, we observed fewer shuttling signals in the absence of Cdc10, but the remaining ones could be detected more easily owing to the absence of signals from the septin filaments (Fig. 4A; Movie 8; see below). This peculiar observation could be explained by homotypic interactions, as observed for Cdc3 from *S. cerevisiae* in the absence of Cdc10 (McMurray et al., 2011). The same interdependency of subcellular septin localization was also observed at basal septa of hyphae and in cytoplasmic rings (Fig. S3D).

To study the interdependency of septins in filaments, we also analysed the localization of Gfp fusion proteins in the absence of the other septins. Whenever one septin was missing the formation of filaments was altered (Fig. S4A). For example, Cdc3–GfpN-containing filaments were shorter and restricted to the region of the initial cell in strains lacking Cdc12 (Fig. S4A).

To further substantiate these findings, we tested septin proteins carrying a deletion in the α0 helix. This region is crucial for the septin interaction at the NC interface and is important for heteromer formation (Bertin et al., 2010; McMurray et al., 2011). The α0 helix is conserved in Cdc3, Cdc10, and Cdc12 but not in Cdc11 (Fig. S3E). Analysing Cdc3α0Δ–GfpN revealed that cytoplasmic rings were no longer formed and septa localization was drastically reduced (Fig. S3F). Moreover, cytoplasmic signals increased whereas, importantly, endosomal signals were strongly reduced (Fig. 4B) indicating that the ability to heterodimerize is important for endosomal localization. There was also an increase of the cytoplasmic signal of Cdc10α0Δ–GfpN but only a weak reduction on endosomes was observed (Fig. 4B). Consistent with this, the presence of Cdc12–GfpN on shuttling endosomes was hardly detectable in strains expressing Cdc3α0Δ (Fig. 4B) suggesting that correct heteromerization is needed for endosomal localization. In case of Cdc10α0Δ, the reduction of Cdc12–GfpN was not as severe (Fig. 4B). Thus, annealing of octamers might not be essential for endosomal localization.

Analysing filament formation revealed that Cdc3α0Δ–GfpN as well as Cdc10α0Δ–GfpN did not form any kind of cortical filaments (Fig. 4C). Consistently, Cdc12–GfpN failed to form filaments if strains expressed either Cdc3α0Δ or Cdc10α0Δ. Thus, heteromeric units are needed to form long extended septin filaments, further supporting the observation that cortical filaments are higher-order structures.

Finally, we tested a strain expressing both Cdc3–GfpC and Cdc12–CherryC, a septin pair carrying C-terminal fusion proteins. This should interfere with C-terminal interactions of Cdc3–Cdc12. The presence of two fluorescently tagged fusion proteins in one strain had no influence on septum localization or formation of cytoplasmic rings. However, endosomal localization of both proteins was almost abolished (Fig. 4D). Thus, when Cdc12 carries a C-terminal extension, endosomal localization of Cdc3–GfpC is severely disturbed supporting the presence of heteromers on the surface of shuttling endosomes. Furthermore, the C-terminal domain appears to be needed for the attachment to endosomes. In conclusion, our *in vivo* evidence indicates that septins form heteromeric building blocks on the surface of shuttling endosomes.

The RNA-binding protein Rrm4 mediates endosomal transport of all septin mRNAs

Previously, we have shown that the key RNA-binding protein Rrm4 mediates endosomal transport of *cdc3* mRNA leading to endosomal transport of Cdc3 protein. Most likely this is achieved by local translation on shuttling endosomes (Baumann et al., 2014, 2015). In control experiments, we verified that loss of septins did not influence microtubule-dependent motility of Rrm4 (Fig. S4B–E).

To test whether Rrm4 mediates transport of all septin mRNAs in order to load endosomes with septin proteins, we performed RNA imaging experiments in live cells using the λN-Gfp system (Fig. 5A) (Baumann et al., 2014, 2015). Analysing septin mRNAs revealed processive movement in all cases (Fig. 5B; Movie 9). The number of processive messenger ribonucleoprotein (mRNP) particles as well as the range and the velocity of movement were comparable for all four mRNAs (Fig. 5C–E).

The transport of septin mRNA was clearly Rrm4 dependent because in the absence of Rrm4 no processive movement was detectable (Fig. 5F,G). This is consistent with early results showing that Rrm4 is the key mRNA-transport protein (Baumann et al., 2014; König et al., 2009).

To extend this study, we analysed *cdc3B*^{16} mRNA in the absence of Cdc12 because, here, Cdc3 protein is no longer present on endosomes (Fig. 4A). However, processive movement of *cdc3B*^{16} mRNA still occurred with a similar range and velocity (Fig. 5B,D,E). We even observed an increase in the number of events of processive movement (Fig. 5C). A possible explanation for the latter would be

Journal of Cell Science (2016) 129, 2778-2792 doi:10.1242/jcs.182824

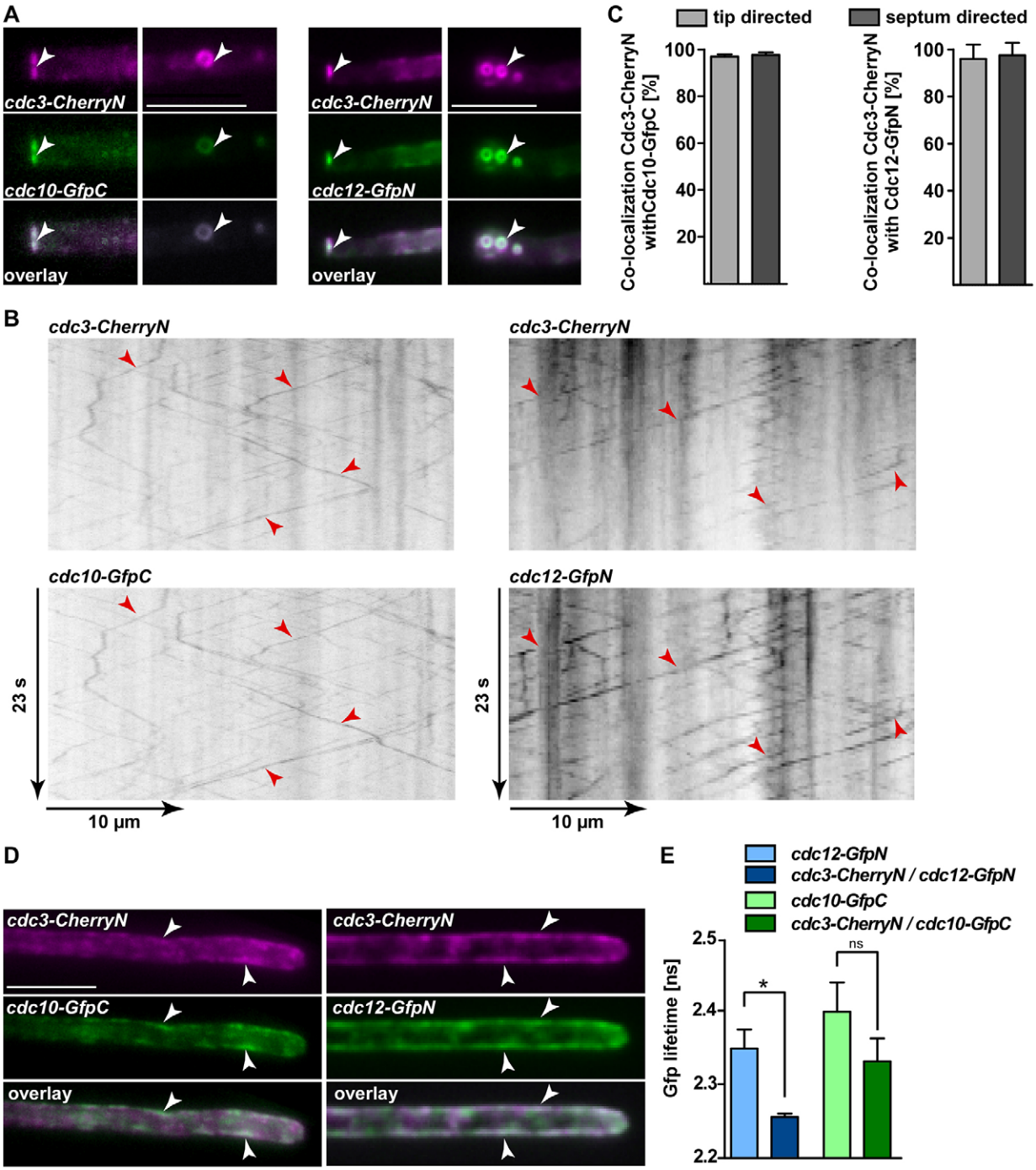

Fig. 3. Cdc3 colocalizes extensively with Cdc10 and Cdc12. (A) Hyphae expressing Cdc3–CherryN (magenta) under the control of the constitutively active promoter P_{otef} and Cdc10–GfpC or Cdc12–GfpN (green) at endogenous levels. Colocalization (overlay, in white with arrowheads indicating regions of colocalization) was analysed at basal septa (left) and cytoplasmic rings (right). Scale bar: 5 µm. (B) Kymographs (dual view technology) analysing colocalization of Cdc3–CherryN (top, inverted image of red fluorescence) and Cdc10–GfpC or Cdc12–GfpN (bottom, inverted image of green fluorescence on shuttling endosomes, red arrowheads; Movies 6,7). (C) Bar diagram showing the percentage of Cdc3–CherryN signals that colocalize with Cdc10–GfpC or Cdc12–GfpN signals. Endosomes moving processively towards the tip or the septum were analysed (error bars represent mean±s.d.; *n*=15 hyphae). (D) Hyphae expressing Cdc3–CherryN (magenta) and Cdc10–GfpC or Cdc12–GfpN (green). Colocalization (overlay, in white with arrowheads indicating regions of colocalization) was analysed in single planes (note that filaments exhibit cortical staining). Scale bars: 5 µm. (E) Bar diagram of Gfp lifetime measured by FLIM microscopy (*n*=3 independent experiments, at least 5 hyphae were analysed per strain and experiment, error bars represent mean±s.e.m.). **P*<0.05; ns, not significant (paired two-tailed *t*-test).

that *cdc3* and *cdc12* mRNA compete for the same binding sites on endosomes. Given that endosomal transport of *cdc3* mRNA can be uncoupled from Cdc3 protein transport, we can exclude the possibility that the translation product Cdc3 binds its own mRNA for autoregulatory purposes (Caballero-Lima et al., 2014; Haag et al., 2015). In essence, all septin mRNAs are transported in an Rrm4-dependent manner on endosomes suggesting endosomal assembly of the translation products.

Journal of Cell Science (2016) 129, 2778-2792 doi:10.1242/jcs.182824

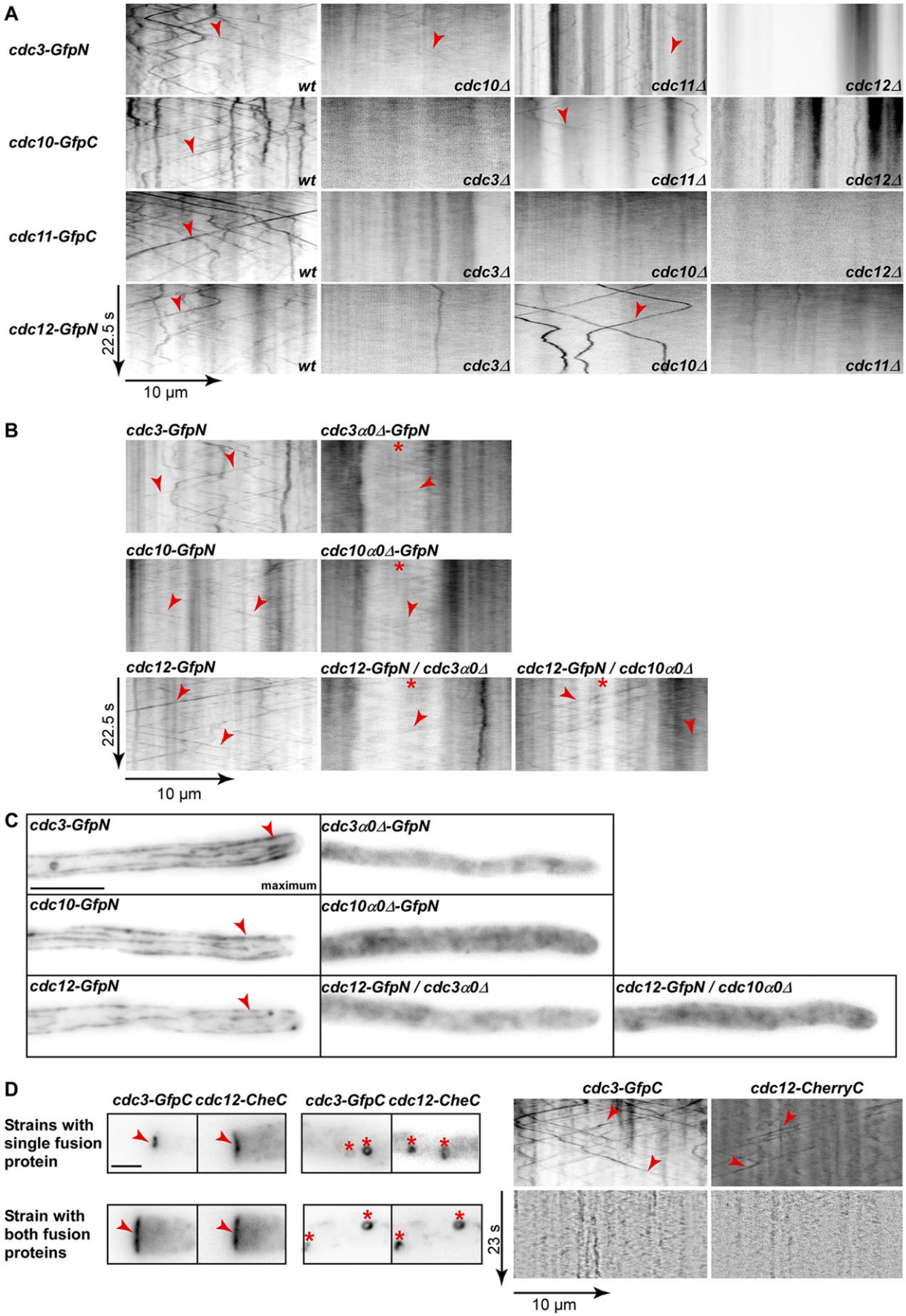

Fig. 4. See next page for legend.

Journal of Cell Science (2016) 129, 2778-2792 doi:10.1242/jcs.182824

Fig. 4. Septins form heteromeric units on shuttling endosomes and in filaments. (A) Kymographs (inverted signals) of strains expressing the septin Gfp fusions indicated on the left. For each septin, one of the three other septin-encoding genes was deleted and tested (Movie 8). Endosomal shuttling (red arrowheads) is affected in most cases. (B) Kymographs (inverted) of strains expressing the septin Gfp fusions indicated in comparison with strains in which the α0 helix is deleted. Red asterisks mark the nuclear region with reduced background signal; red arrowheads indicate shuttling units. (C) Micrographs of hyphae expressing Gfp fused to the septin indicated (maximum intensity projections) in comparison to strains with deleted α0 helix. Red arrowheads indicate septin filaments. Scale bar: 10 µm. (D) Micrographs of strains expressing Cdc3–GfpC and Cdc12–mCherryC either individually (top) or simultaneously (bottom); septa localization (left), cytoplasmic ring localization (middle) and endosomal localization (kymographs, right) is shown. Red arrowheads indicate septa (left) or shuttling endosomes (right); red asterisks mark cytoplasmic rings.

Rrm4 is essential for septin localization on endosomes

Next, we addressed whether the endosomal localization of septin proteins is also dependent on Rrm4 (Baumann et al., 2014). To this end we initially demonstrated that Cdc3–GfpN and Cdc12–GfpN colocalized almost exclusively with Rrm4–CherryC (a functional C-terminal fusion protein, Baumann et al., 2012) on shuttling units (Fig. 6A,B; Movie 10). This indicates that both septins are present on Rrm4-positive endosomes (Baumann et al., 2014).

Studying Cdc3–GfpN and Cdc12–GfpN in *rrm4Δ* strains showed that the localization of both septins to septa and cytoplasmic rings was not altered (Fig. S4F), but the endosomal localization was lost (Fig. 6C). This holds true for a strain expressing Cdc12–GfpN and lacking Cdc10 as well as Rrm4, suggesting that, in this case, endosomal localization of Cdc12–GfpN also needed Rrm4 (Fig. 6C). Thus, endosomal septin localization is dependent on the mRNA-transport protein Rrm4 further supporting the hypothesis of endosomal translation and assembly of septin proteins.

Septins are co-delivered by endosomes

So far we have shown that all septin mRNAs and encoded proteins are transported on endosomes. This might be needed for efficient formation of higher-order cortical filaments at the growing pole. Initially, we focused on Cdc3–GfpN because it exhibited the best biological activity, and in previous studies we have demonstrated in fluorescence recovery after photobleaching (FRAP) experiments that recovery of Cdc3–GfpN depends on Rrm4 (Baumann et al., 2014; Pohlmann et al., 2015). In this study, we were able to increase the spatial resolution and could resolve cortical filaments. We observed that Cdc3–GfpN signals recovered in the same cortical area that was present before bleaching. Interestingly, the recovery took place over the entire cortical area and not only at the end of higher-order filaments (Fig. 7A). The same is true for the recovery of the Cdc3–GfpN signal in the absence of Rrm4, but in this case the extent of recovery was strongly reduced (Fig. 7A,B). Thus, Rrm4-dependent endosomal transport of Cdc3 promotes its efficient assembly in cortical filaments at the growth pole.

Finally, we aimed to address whether heteromeric septin signals recover at identical subcellular sites. To this end, we performed dual-colour 3D photobleaching experiments. At 5 min after dual-colour bleaching, we observed simultaneous recovery of Cdc3–CherryN and Cdc12–GfpN at identical subcellular sites, suggesting that heteromeric units are assembled in cortical septin filaments (Fig. 7C). In addition, 3D photobleaching experiments demonstrated that the recovery of both fluorescence signals was dependent on Rrm4 (Fig. 7D), although recovery of Cdc3–CherryN was less prominent. This is likely due to the photophysical properties of mCherry causing extensive bleaching during acquisition of *z*-planes (12 sections) at two different time points (see Materials and Methods). Therefore, the statistical analysis revealed a significant difference only for Cdc12–GfpN (Fig. 7D). Importantly, FRET experiments revealed that without Rrm4, the interaction of Cdc3–CherryN with Cdc12–GfpN is strongly reduced (Fig. 7E). This is most likely due to the lack of endosomal assembly and transport (see above). In summary, the *in vivo* data presented here substantiate the hypothesis that heteromeric septin building blocks are transported on endosomes to enhance formation of higher-order septin filaments at the growth pole of hyphae.

DISCUSSION

Septins are highly versatile cytoskeletal components that form various higher-ordered structures such as rings and filaments at distinct subcellular sites (Bridges and Gladfelter, 2015; Fung et al., 2014). At present it is unclear how the underlying intracellular trafficking of septins subunits is orchestrated. Furthermore, in fungal hyphae it was questionable whether the observed higher-order cortical filaments consist of the known heteromeric septin subunits containing of all four septins, because Cdc11 and Cdc12 could, so far, not be detected in filaments (Alvarez-Tabares and Perez-Martin, 2010).

Here, we present a comprehensive genetic and cell biological study in *U. maydis* using N-and C-terminally Gfp-tagged versions of all known septins, while preserving endogenous expression levels and regulatory RNA elements. We demonstrate that all four septins are present in cortical filaments and provide detailed *in vivo* evidence to support the hypothesis of endosomal assembly and transport of septin subunits.

Cellular functions of septins in *U. maydis*

Previous analysis of deletion mutants in *U. maydis* revealed that septins were crucial for correct cell morphology but dispensable for cytokinesis of yeast cells (Alvarez-Tabares and Perez-Martin, 2010; Boyce et al., 2005). In contrast to studies in human pathogens such as *Cryptococcus neoformans* and *Candida albicans* (Kozubowski and Heitman, 2010; Warenda et al., 2003), loss of septins did not affect plant virulence of *U. maydis* (Alvarez-Tabares and Perez-Martin, 2010). Here, we observe that all four septin deletion mutants exhibited comparable defects in hyphal growth, providing genetic evidence that they function together in a complex. Loss of each septin causes the delayed formation of hyphal septa similar to that seen in *A. nidulans* (Hernandez-Rodriguez et al., 2012). Furthermore, all septins are crucial for establishment of unipolar growth as well as for unconventional secretion of Cts1 (Stock et al., 2012). Thus, septins appear to be particularly important for the efficient execution of the hyphal growth programme.

Assembly of septins in higher-order cortical filaments

Like in mammalian cells, extended septin filaments are present at the cortex of fungal hyphae (Kaufmann and Philippsen, 2009; Khan et al., 2015; Kozubowski and Heitman, 2010). In *U. maydis*, filaments containing Cdc3 or Cdc10 were found in yeast-like growing cells and hyphae (Alvarez-Tabares and Perez-Martin, 2010; Baumann et al., 2014; Böhmer et al., 2009). We observed that all septins form cortical filaments consisting of heteromeric subunits. However, in contrast to their endosomal localization, the localization in filaments is affected by modifications of the N- or C-termini. This might be one reason why heteromeric septin filaments have not previously been reported in fungi. For example, the N-terminal fusion protein Cdc11–GfpN does not assemble in filaments (this work; Alvarez-Tabares and Perez-Martin, 2010)

Journal of Cell Science (2016) 129, 2778-2792 doi:10.1242/jcs.182824

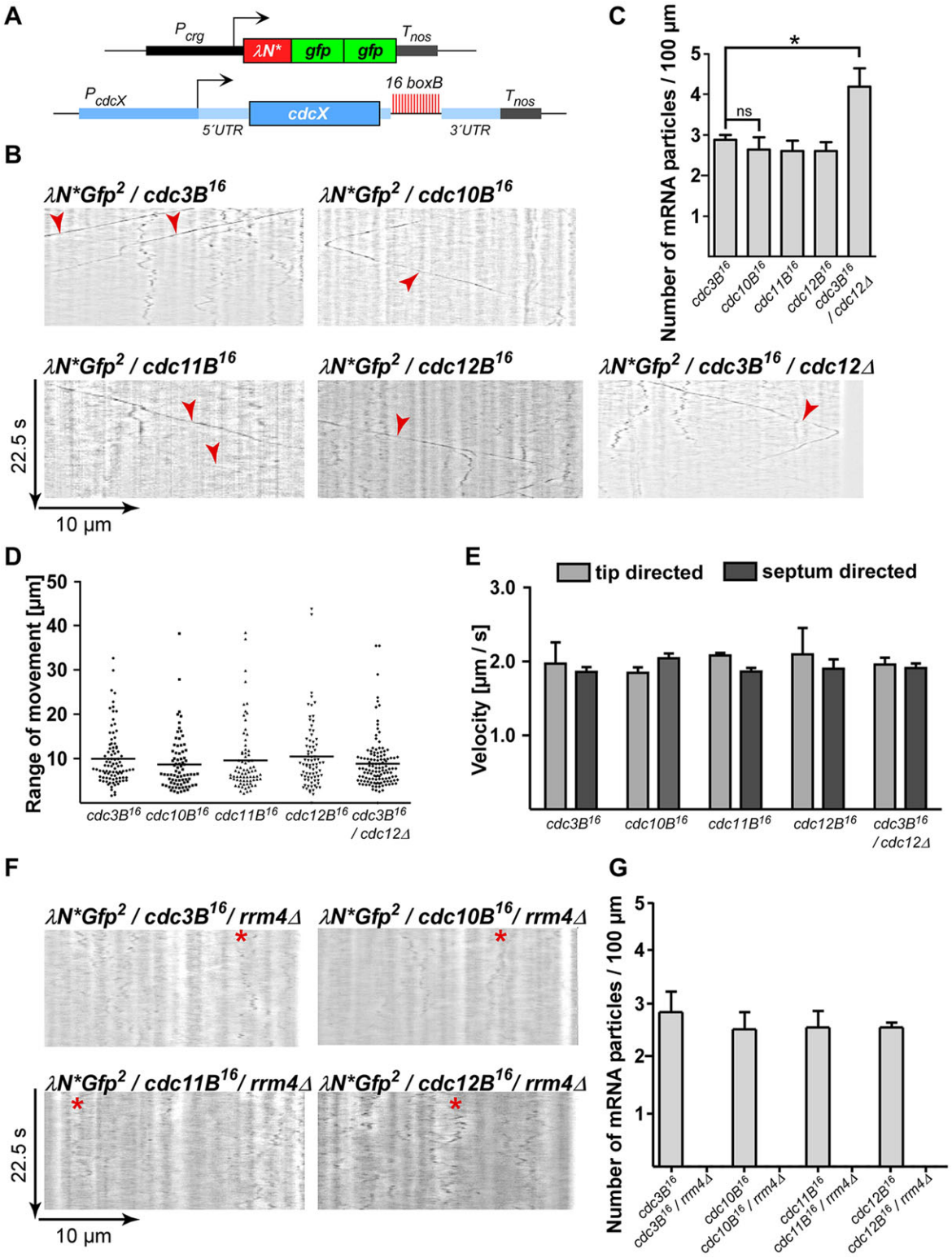

Fig. 5. Endosomal shuttling of septin mRNA is dependent on Rrm4. (A) Components of the λN*Gfp RNA reporter system (P_{crg1}, arabinose-regulated promoter; T_{nos}, heterologous transcriptional terminator; *cdcX*, septin gene carrying 16 copies of *boxB* hairpin in its 3′ UTR, Baumann et al., 2014). λN*Gfp^2 is recruited to mRNAs containing the λN*-binding sites designated *boxB* (Baumann et al., 2014, 2015). (B) Kymographs of hyphae expressing the λN*Gfp^2 protein and *boxB*-containing septin mRNAs (red arrowheads indicate processively moving particles; Movie 9). (C) Bar diagram showing the number of processively moving particles normalized to 100 µm (n=3 independent experiments, at least 10 hyphae per experiment, error bars represent mean±s.e.m.). *P<0.05; ns, not significant; unpaired two-tailed t-test. (D) Diagram indicating the range of processive movement (at least 30 hyphae per strain). (E) Bar diagram showing the velocity of processively moving mRNP particles either to the tip or towards the septum (n=3 independent experiments, at least 10 hyphae per experiment, error bars represent mean± s.e.m.). (F) Kymographs of a hypha expressing the λN*Gfp^2 protein and *boxB*-containing septin mRNAs with an additional deletion of *rrm4* (red asterisks indicate static particles or corralled movement). (G) Bar diagram showing the number of processively moving particles normalized to a 100 µm length in the septin mRNA strain indicated in comparison to *rrm4* deletion strains (n=3 independent experiments, at least 5 hyphae per experiment, error bars represent mean±s.e.m.).

Journal of Cell Science (2016) 129, 2778-2792 doi:10.1242/jcs.182824

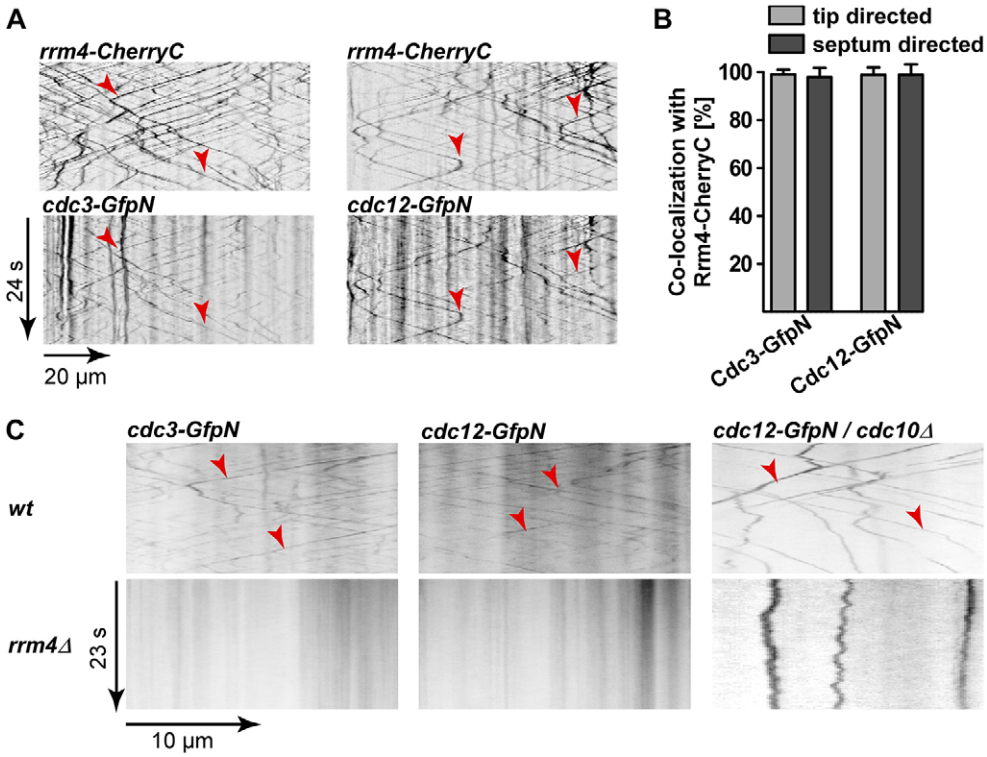

Fig. 6. Loss of Rrm4 abolishes septin localization on shuttling endosomes. (A) Kymographs analysing colocalization in strains expressing both Rrm4–CherryC (top, inverted image of red fluorescence) and either Cdc3–GfpN (bottom left) or Cdc12–GfpN (bottom right, inverted image of green fluorescence; Movie 10). Red arrowheads mark examples of colocalizing signals on shuttling endosomes. Note that the vertical lines in the kymographs of septin fusion proteins are not static endosomes, but they are due to the localization of septins in cortical structures. (B) Bar diagram showing the percentage of Cdc3–GfpN and Cdc12–GfpN signals that colocalize with Rrm4–CherryC signals. Endosomes moving processively towards the tip or the septum were analysed (error bars represent mean± s.d.; *n*=15 hyphae). (C) Kymographs of strains expressing Cdc3–GfpN (left) and Cdc12–GfpN (middle and right, note that in the strain on the right the *cdc10* gene is deleted). Red arrowheads mark examples of shuttling endosomes. Bottom panels show kymographs of strains carrying an additional deletion in *rrm4*.

whereas the C-terminal fusion does (this work). Hence, a careful and comprehensive analysis of their localization was needed.

Based on the fact that septin filaments bundle laterally (DeMay et al., 2011; Fung et al., 2014) and that they are most likely in register with adjacent filaments (Kaplan et al., 2015), we propose that bundles of heteromeric septin filaments are also formed in *U. maydis* (Fig. 8). Consistent with this, we noticed that the assembly of septins in cortical filaments depends on the different subunits. The heteromeric nature of the cortical filaments was further supported by the observation that the α0Δ mutations, which affect the NC interface of Cdc3 with Cdc12, and Cdc10 with itself, abolish filament formation. Furthermore, colocalization experiments showed that Cdc3 and Cdc12 fluorescence recovered simultaneously at distinct sites in the filament, strongly arguing for the incorporation of heteromeric subunits. Formation of filament bundles requires intimate interactions of septin subunits. In accordance, certain fusion proteins such as C-terminally tagged Cdc3 and Cdc12 are impaired in filament formation. This could be due to a disturbed interaction with other septins or with potential septin scaffolding proteins (Sadian et al., 2013).

Previously, it has been reported that heterooctameric septin subunits anneal head-to-tail to form longer filaments only from the ends (Bridges et al., 2014). We observed that recovery occurs over the complete length of the filament. A possible explanation for this apparent discrepancy is that we might mainly detect the lateral assembly of septin filaments forming bundles and not the annealing process itself (DeMay et al., 2011). A pronounced bundling of septin filaments at the growth pole would explain the observed gradient (Fig. 8).

At present we can only speculate about the detailed function of septin filaments for efficient hyphal growth of *U. maydis*. It has been shown that Cdc10 colocalizes with a sub-set of microtubules (Alvarez-Tabares and Perez-Martin, 2010) indicating that septins could regulate microtubule dynamics during hyphal growth, for example, by specific post-translational modifications (Spiliotis et al., 2008).

Heteromeric septin subunits on the cytoplasmic surface of endosomes

Previous studies have already reported a close link between septin assembly and membranes (Bezanilla et al., 2015; Garcia et al., 2016; Heasley and McMurray, 2016). Using membrane bilayers and liposomes it was initially discovered that the polybasic region interacts with membrane lipids (Casamayor and Snyder, 2003; Zhang et al., 1999) and enhances rod formation (Bertin et al., 2010; Tanaka-Takiguchi et al., 2009). Moreover, these rods diffuse on membranes in two dimensions promoting the annealing process, which results in the formation of higher-order septin structures (Bridges et al., 2014). The finding that Cdc3 and Cdc12 are present on shuttling endosomes raised the intriguing possibility that heteromeric septin subunits are assembled on endosomes (Baumann et al., 2014).

Now, we show that all four septins are present on shuttling Rrm4-positive endosomes. Endosomal localization was not affected by N- or C-terminal fusion proteins, suggesting that no higher-ordered structures are assembled on their surface. Analysis of deletion mutants revealed that endosomal localization of septins was interdependent on each of the individual septins. This was further verified by analysing the aforementioned α0Δ mutations. Cdc3α0Δ was hardly detectable on endosomes and caused a clear reduction in the endosomal localization of Cdc12. Consistent with this, if both proteins carry a C-terminal fusion protein, none of them localize to endosomes, suggesting the formation of Cdc3–Cdc12 heteromers. Endosomal localization of Cdc10α0Δ was only reduced and therefore its influence on Cdc12 localization was not as drastic. Hence, the interaction at the NC interface of Cdc10 with itself appears to be unessential for endosomal localization. Taken

Journal of Cell Science (2016) 129, 2778-2792 doi:10.1242/jcs.182824

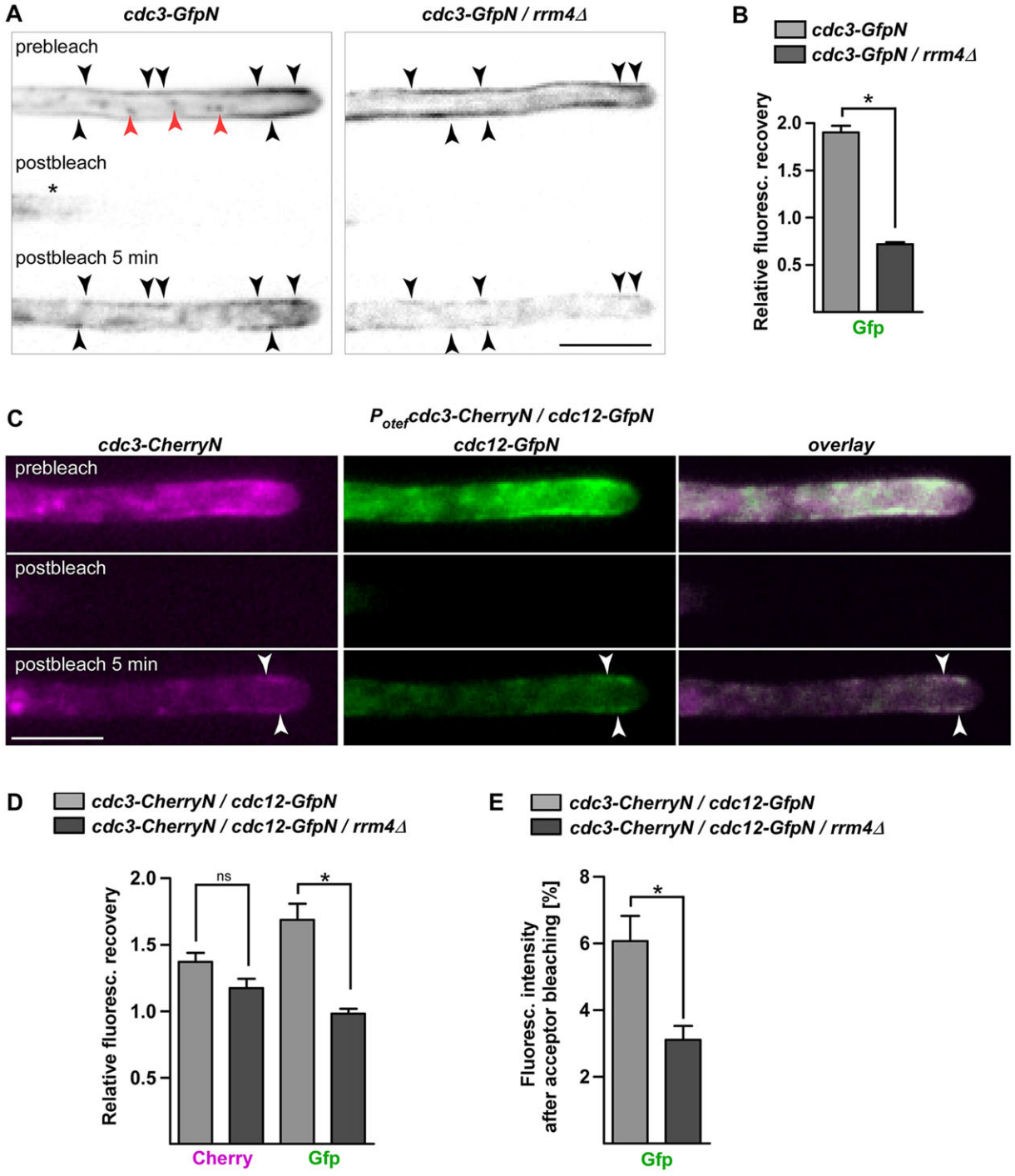

Fig. 7. Rrm4 is needed for efficient recovery of Cdc3 and Cdc12 in septin filaments. (A) Representative 3D photobleaching experiment analysing hypha expressing Cdc3–GfpN (left) in comparison to a similar *rrm4Δ* strain (right; filled arrowheads, septin filaments; red arrowheads, endosomes). Scale bar: 5 µm. (B) Bar diagram of 3D photobleaching experiment (n=3 independent experiments; at least 5 hyphae were analysed per experiment, error bars represent mean± s.e.m.). *P<0.05, paired two-tailed t-test. (C) Representative 3D photobleaching experiment showing hyphal tips expressing Cdc12–GfpN (green) and Cdc3–CherryN (magenta). Colocalization (overlay, in white with arrowheads indicating regions of colocalization) was analysed before and 5 min after bleaching. Scale bar: 5 µm. (D) Bar diagram of 3D photobleaching experiments exhibiting recovery of mCherry or Gfp fluorescence as indicated (n=3 independent experiments, at least 5 hyphae were analysed per experiment; error bars represent mean±s.e.m.). *P<0.05; ns, not significant (paired two-tailed t-test). (E) Bar diagram of FRET experiments showing Gfp fluorescence after acceptor bleaching with and without the presence of Rrm4 as indicated (n=3 independent experiments, at least 5 hyphae were analysed per strain and experiment, error bars represent mean±s.e.m.); *P<0.05 (paired two-tailed t-test).

together, we conclude that heteromeric subunits are formed on the surface of endosomes (Fig. 8), but the exact heteromeric composition such as dimers, tetramers or octamers needs to be addressed further.

Endosome-coupled translation for septin assembly

We propose that local translation of septin mRNAs mediates endosomal assembly of septin heterooligomers (Fig. 8). This idea is based on our previous study showing that Cdc3 protein and mRNA

Journal of Cell Science (2016) 129, 2778-2792 doi:10.1242/jcs.182824

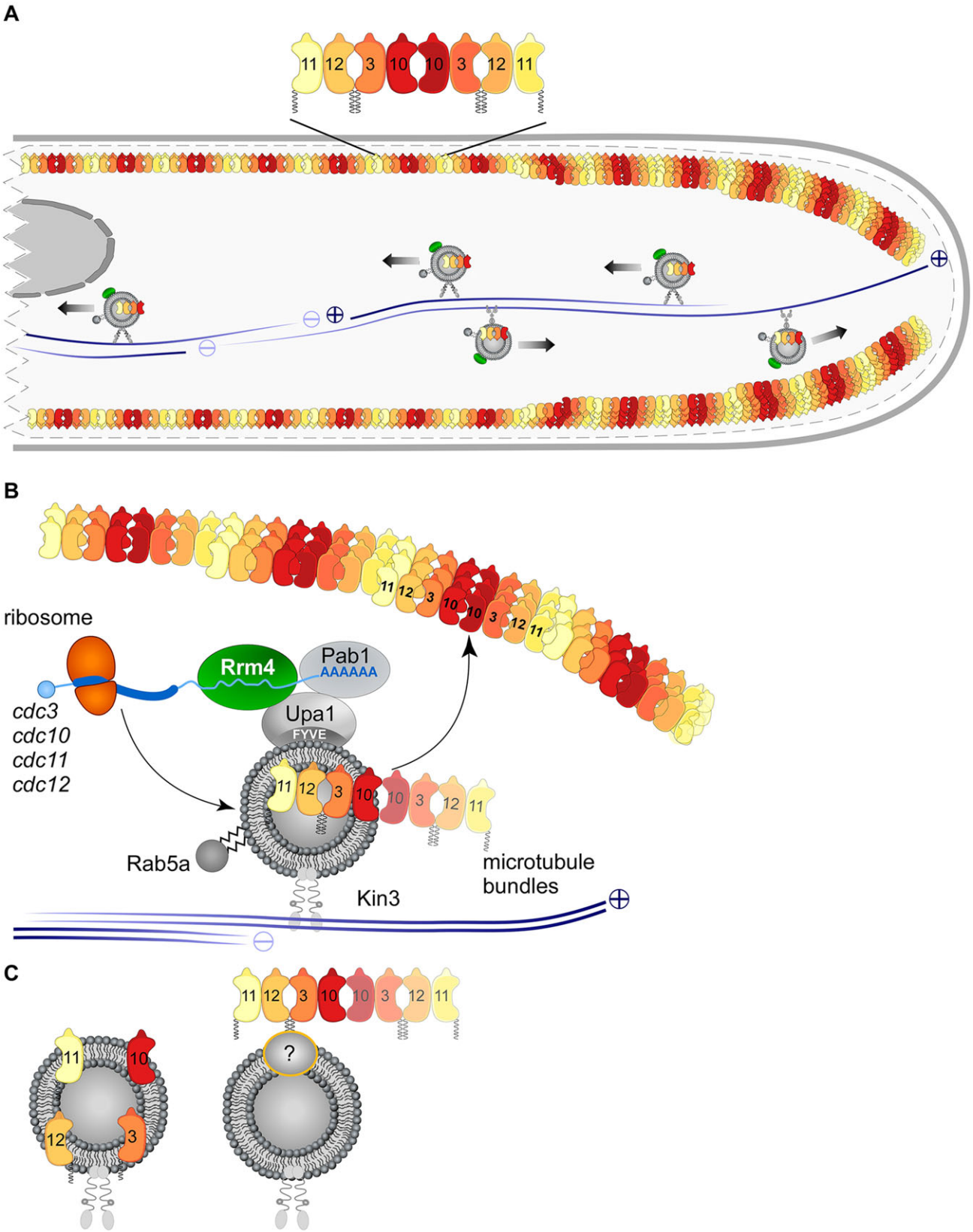

Fig. 8. Heteromeric septin complexes are assembled on shuttling endosomes for transport and formation of higher-order structures. (A) Schematic drawing of a hypha (growth pole at the right, nucleus in grey). Depicted are cortical septin filaments formed by septin heterooctamers (enlarged) that consist of Cdc11–Cdc12–Cdc3–Cdc10–Cdc10–Cdc3–Cdc12–Cdc11. An array of antiparallel microtubules with shuttling endosomes is depicted in the centre. (B) Enlargement of an Rrm4-positive endosome transporting septin mRNAs that are translated by ribosomes during transport. This results in heteromer formation on the surface of endosomes. (C) Two different scenarios explaining the presence of septins on endosomes. The interdependency of the septins for endosomal localization favours the right-hand model. A potential adaptor protein linking septins to endosomes is indicated by a question mark. Further details are given in the text.

Journal of Cell Science (2016) 129, 2778-2792 doi:10.1242/jcs.182824

colocalize on endosomes and that without mRNAs or ribosomes on endosomes the translation product Cdc3 is absent (Baumann et al., 2014; Haag et al., 2015; Jansen et al., 2014). This is supported by the finding that Rrm4-positive endosomes transport translationally active ribosomes (Higuchi et al., 2014; Palacios, 2014).

We could demonstrate in this study that all septin mRNAs are transported on endosomes. Furthermore, Rrm4 is essential for the endosomal localization of the analysed septin proteins Cdc3 and Cdc12. These results clearly demonstrate that those heteromeric septin subunits that are formed in the absence of Rrm4 are unable to localize to endosomes. Thus, without septin mRNA on endosomes, heteromeric subunits cannot bind endosomes. Importantly, dual-colour 3D photobleaching and basic FRET experiments demonstrate that loss of Rrm4 affects the interaction of Cdc3 and Cdc12 *in vivo*. This shows that septin subunits can be formed without endosomal transport, but less efficiently.

Interestingly, due to the septin interdependency mentioned above, local translation of septin mRNAs seems insufficient for endosomal attachment of the translation products. An attractive explanation would be that, compared to single septin proteins, heterooligomers bind endosomal lipids stronger. This could be due to an increased avidity of membrane binding, for example, mediated by the multiplication of polybasic regions in septin oligomers, or the ability of septin oligomers to recognize membrane curvature (Bridges et al., 2016). Alternatively, an interaction partner that specifically interacts with the C-termini of Cdc3 and Cdc12 might be present. This is supported by our finding that Cdc3 and Cdc12 lose endosomal localization when both proteins carry a C-terminal fusion protein (Fig. 8). In summary, local translation and assembly of the newly synthesized proteins most likely function together in endosomal tethering of septins to coordinate their transport.

Conclusion

Details on the mechanism of intracellular septin trafficking have not yet been clarified. It is unknown, for example, how septins reach dendritic spines, the base of the sperm cell annulus or the base of cilia (Mostowy and Cossart, 2012; Saarikangas and Barral, 2011). Here, we present *in vivo* evidence that septin heteromeric subunits are assembled and transported on endosomes for filament formation and efficient hyphal growth (Fig. 8). Local translation during septin assembly might even explain how more complex septin filaments could be assembled in humans, which contain 13 different septin-encoding genes with numerous splice products (Barral, 2010; Spiliotis and Gladfelter, 2012). A defined septin heterooligomer consisting of distinct septin subunits could elegantly be produced by local translation of the individual septins at identical subcellular sites. The fact that septins have been found in neuronal vesicles and vesicle-like structures (Beites et al., 1999; Xie et al., 2007) opens the intriguing possibility that not only septin structures are conserved, but potentially also the intimate link to membrane trafficking for assembly and transport.

MATERIALS AND METHODS

Standard molecular biology techniques, strain generation and accession numbers

Standard procedures for plasmid and strain generations were used as described elsewhere (Brachmann et al., 2004; Loubradou et al., 2001; see Tables S1–S4). Proteins were tagged with eGfp, the enhanced version of green fluorescent protein (Clontech, Mountain View, CA), or mCherry, a derivate of mRfp (monomeric red fluorescent protein). Accession numbers of *U. maydis* genes used in this study: *rrm4* (UMAG_10836), *cdc3* (UMAG_10503), *cdc10* (UMAG_10644), *cdc11* (UMAG_03449), *cdc12* (UMAG_03599), *cts1* (UMAG_10419).

Fluorometric measurement of endochitinolytic activity

Determination of Cts1 activitiy in the supernatant of cells was performed in a similar manner to in previous studies (Koepke et al., 2011; Langner et al., 2015). Note that *U. maydis* cells were grown at 20°C in order to prevent morphological defects. At least three independent biological experiments were performed with three technical replicates per strain.

Microscopy, dual-colour imaging, image processing and quantification

Laser-based epifluorescence-microscopy was performed on a Zeiss Axio Observer.Z1 as previously described (Baumann et al., 2014, 2015, 2016; Pohlmann et al., 2015). Colocalization studies of dynamic processes were carried out by applying msALEX (millisecond alternating laser excitation; Baumann et al., 2015) or with a two-channel imager (DV2, Photometrics, Tucson, AZ, USA; Pohlmann et al., 2015; Baumann et al., 2016). Yeast-like cells of all septin deletion strains were incubated at 20°C in order to prevent morphological defects (Alvarez-Tabares and Perez-Martin, 2010). To visualize septin localization at septa, in rings or in filaments, *z*-stacks with an exposure time of 150 ms/plane and a *z*-distance of 0.23 µm were recorded. All parts of the microscope systems were controlled by the software package Metamorph (Version 7.7; Molecular Devices).

RNA imaging in live cells, FM4-64 staining and benomyl treatment

RNA imaging in live cells and subsequent data analysis was performed as previously described (Baumann et al., 2012, 2014). Per strain and experiment, >10 hyphae were analysed. Statistical tests were performed using Prism5 (Graphpad, La Jolla, CA). Staining of hyphae with FM4-64 and benomyl treatment was performed as described previously (Baumann et al., 2012; Becht et al., 2006).

3D photobleaching experiments

For 3D photobleaching experiments, a 100× Plan-Neofluar objective (NA 1.3; Zeiss) and a 472 nm LED (CoolLED, precisExcite, Andover, UK) to excite Gfp fluorescence were used. An area of 15 µm from hyphal tips was bleached with 33% laser power of a 405 nm laser (80 mW fibre output, beam diameter 16 pixels, bleach time 5 ms/pixel). Bleaching was carried out in 18 *z*-planes with a *z*-distance of 0.3 µm. Fluorescence recovery was detected directly after bleaching and 5 min later, with an exposure time of 350 ms/plane in a *z*-stack of 18 planes with a *z*-distance of 0.3 µm. This time-point was chosen based on previous FRAP experiments carried out with a comparable set-up (Baumann et al., 2014). For data analysis, *z*-planes were merged to maximum intensity projections and the average background was subtracted. Fluorescence intensity after bleaching was set to 0 and the fluorescence recovery 5 min after bleaching was calculated. Intensity values were not corrected for acquisition bleaching as we were only interested in a relative readout of the fluorescence recovery. Statistical tests were performed using Prism5 (Graphpad).

Dual-colour 3D photobleaching

3D photobleaching experiments in the colocalization strain were carried out using dual-view technology. The laser for excitation of Gfp (488 nm/100 mW) was set to 15% and the laser for excitation of mCherry (561 nm/150 mW) was set to 20%. The same area and bleaching settings were used as described above (12 *z*-planes; *z*-distance of 0.2 µm, exposure time of 500 ms/plane). Recovery of mCherry was strongly affected by acquisition bleaching. Data analysis was performed as described above.

FRET after acceptor bleaching

For intensity-based FRET measurements, the initial Gfp fluorescence signal was acquired with an exposure time of 100 ms/plane (*z*-stack of 13 planes, *z*-distance of 0.3 µm, 488 nm laser line). Acceptor bleaching of mCherry was performed with an exposure time of 5 s/plane using the 561-nm laser line. The Gfp fluorescence after acceptor bleaching was acquired with the same settings described above. For analysis, a sum projection of *z*-planes was made and a maximum background subtraction was performed. The apparent FRET efficiency was calculated using the following formula: $E_{FRET}=(\text{intensity}_{after}-\text{intensity}_{before})/\text{intensity}_{after}\times 100$. Note that a region

of 696×520 pixels was analysed in total, corresponding to about 30 µm of the hyphal tip. Statistical tests were performed using Prism5 (Graphpad).

FLIM

FLIM was performed on a confocal laser scanning microscope (Zeiss LSM 780) additionally equipped with a single-photon counting device with picosecond time resolution (Hydra Harp 400, PicoQuant, Berlin, Germany). Gfp fluorescence was excited at 485 nm using a linearly polarized diode laser (LDH-D-C-485) operated at a repetition rate of 32 MHz. Excitation power was set to 1 µW at the objective (40× water immersion, Zeiss C-PlanApo, NA 1.2). The emitted light was collected in the same objective and separated into its perpendicular and parallel polarization (Thorlabs PBS 101, Thorlabs GmbH, Germany). Fluorescence was then detected by Tau-SPADs (PicoQuant) in a narrow range of the emission spectrum of Gfp (band-pass filter, HC520/30 AHF). Images were taken with a 12.6-µs pixel time and a resolution of 110 nm/pixel (Zoom 3,9; 520×80). A series of 40 frames was merged into one image to increase photon numbers per pixel.

Single-pixel fluorescence lifetime analysis

The fluorescence lifetime of Gfp was analysed using the software tool SymPhoTime 64, version 2.0 (PicoQuant, Berlin, Germany). Owing to the low excitation power to prevent photobleaching during image acquisition and the small pixel size to gain spatial resolution, the number of photons per pixel was still low after merging of frames, ranging from 300 to 2000 photons per pixel. Therefore, we applied a fit model with a minimal number of parameters to the data, in conjunction with a maximum likelihood estimator (MLE, Stahl et al., 2013; Weidtkamp-Peters et al., 2009). We used a bi-exponential model function with two fluorescence lifetimes τ_1 and τ_2, background contribution and correction for shifting of the instrument response function. The same model was applied to the donor-only and FRET-data sets. Thus, the decay histogram of eGFP is approximated in the subsequent fluorescence lifetime analysis by an intensity-weighted average lifetime $\tau_{Av\ Int}$.

Acknowledgements

We acknowledge Drs K. Schipper, V. Göhre, U. Fleig and laboratory members for discussion and reading of the manuscript. We are grateful to U. Gengenbacher and S. Esch for excellent technical assistance. Thanks to Dr R. Kahmann from the Max Planck Institute for Terrestrial Microbiology for support.

Competing interests

The authors declare no competing or financial interests.

Author contributions

S.B. and S.Z. were responsible for conception and design, acquisition of data, analysis and interpretation of data, and drafting or revising the article; S.W.-P. was responsible for acquisition of data, and analysis and interpretation of data; M.F. was responsible for conception and design, analysis and interpretation of data, and drafting or revising the article.

Funding

This study was supported by grants from the Deutsche Forschungsgemeinschaft [grant numbers EXC 1028, DFG FE448/9-1 (to M.F.) and CRC1208 (to S.W.P. and M.F.)]; and the iGRAD Molecules of Infection (MOI) programme to S.Z.

Supplementary information

Supplementary information available online at
http://jcs.biologists.org/lookup/doi/10.1242/jcs.182824.supplemental

References

Alvarez-Tabares, I. and Perez-Martin, J. (2010). Septins from the phytopathogenic fungus *Ustilago maydis* are required for proper morphogenesis but dispensable for virulence. *PLoS ONE* **5**, e12933.

Barral, Y. (2010). Septins at the nexus. *Science* **329**, 1289-1290.

Baumann, S., Pohlmann, T., Jungbluth, M., Brachmann, A. and Feldbrügge, M. (2012). Kinesin-3 and dynein mediate microtubule-dependent co-transport of mRNPs and endosomes. *J. Cell Sci.* **125**, 2740-2752.

Baumann, S., König, J., Koepke, J. and Feldbrügge, M. (2014). Endosomal transport of septin mRNA and protein indicates local translation on endosomes and is required for correct septin filamentation. *EMBO Rep.* **15**, 94-102.

Baumann, S., Takeshita, N., Grün, N., Fischer, R. and Feldbrügge, M. (2015). Live cell imaging of endosomal trafficking in fungi. In *Methods in Mol. Biol.: Membrane trafficking*, vol. 1270 (ed. B. L. Tang), pp. 347-363. New York: Springer.

Baumann, S., Zander, S., Weidtkamp-Peters, S. and Feldbrügge, M. (2016). Live cell imaging of septin dynamics in *Ustilago maydis*. In *Methods in Cell Biology: Septins* (ed. A. S. Gladfelter). Elsevier, **136** (in press).

Becht, P., Vollmeister, E. and Feldbrügge, M. (2005). Role for RNA-binding proteins implicated in pathogenic development of *Ustilago maydis*. *Euk. Cell* **4**, 121-133.

Becht, P., König, J. and Feldbrügge, M. (2006). The RNA-binding protein Rrm4 is essential for polarity in *Ustilago maydis* and shuttles along microtubules. *J. Cell Sci.* **119**, 4964-4973.

Beise, N. and Trimble, W. (2011). Septins at a glance. *J. Cell Sci.* **124**, 4141-4146.

Beites, C. L., Xie, H., Bowser, R. and Trimble, W. S. (1999). The septin CDCrel-1 binds syntaxin and inhibits exocytosis. *Nat. Neurosci.* **2**, 434-439.

Bertin, A., McMurray, M. A., Thai, L., Garcia, G., III, Votin, V., Grob, P., Allyn, T., Thorner, J. and Nogales, E. (2010). Phosphatidylinositol-4,5-bisphosphate promotes budding yeast septin filament assembly and organization. *J. Mol. Biol.* **404**, 711-731.

Bezanilla, M., Gladfelter, A. S., Kovar, D. R. and Lee, W.-L. (2015). Cytoskeletal dynamics: a view from the membrane. *J. Cell Biol.* **209**, 329-337.

Böhmer, C., Ripp, C. and Bölker, M. (2009). The germinal centre kinase Don3 triggers the dynamic rearrangement of higher-order septin structures during cytokinesis in *Ustilago maydis*. *Mol. Microbiol.* **74**, 1484-1496.

Booth, E. A., Vane, E. W., Dovala, D. and Thorner, J. (2015). A Forster Resonance Energy Transfer (FRET)-based system provides insight into the ordered assembly of yeast septin hetero-octamers. *J. Biol. Chem.* **290**, 28388-28401.

Boyce, K. J., Chang, H., D'Souza, C. A. and Kronstad, J. W. (2005). An *Ustilago maydis* septin is required for filamentous growth in culture and for full symptom development on maize. *Eukaryot. Cell* **4**, 2044-2056.

Brachmann, A., Weinzierl, G., Kämper, J. and Kahmann, R. (2001). Identification of genes in the bW/bE regulatory cascade in *Ustilago maydis*. *Mol. Microbiol.* **42**, 1047-1063.

Brachmann, A., König, J., Julius, C. and Feldbrügge, M. (2004). A reverse genetic approach for generating gene replacement mutants in *Ustilago maydis*. *Mol. Gen. Genom.* **272**, 488.

Bridges, A. A. and Gladfelter, A. S. (2014). Fungal pathogens are platforms for discovering novel and conserved septin properties. *Curr. Opin. Microbiol.* **20**, 42-48.

Bridges, A. A. and Gladfelter, A. S. (2015). Septin form and function at the cell cortex. *J. Biol. Chem.* **290**, 17173-17180.

Bridges, A. A., Zhang, H., Mehta, S. B., Occhipinti, P., Tani, T. and Gladfelter, A. S. (2014). Septin assemblies form by diffusion-driven annealing on membranes. *Proc. Natl. Acad. Sci. USA* **111**, 2146-2151.

Bridges, A. A., Jentzsch, M. S., Oakes, P. W., Occhipinti, P. and Gladfelter, A. S. (2016). Micron-scale plasma membrane curvature is recognized by the septin cytoskeleton. *J. Cell Biol.* **213**, 23-32.

Caballero-Lima, D., Hautbergue, G. M., Wilson, S. A. and Sudbery, P. E. (2014). In *Candida albicans* hyphae, Sec2p is physically associated with *SEC2* mRNA on secretory vesicles. *Mol. Microbiol.* **94**, 828-842.

Casamayor, A. and Snyder, M. (2003). Molecular dissection of a yeast septin: distinct domains are required for septin interaction, localization, and function. *Mol. Cell. Biol.* **23**, 2762-2777.

DeMay, B. S., Bai, X., Howard, L., Occhipinti, P., Meseroll, R. A., Spiliotis, E. T., Oldenbourg, R. and Gladfelter, A. S. (2011). Septin filaments exhibit a dynamic, paired organization that is conserved from yeast to mammals. *J. Cell Biol.* **193**, 1065-1081.

Dolat, L., Hu, Q. and Spiliotis, E. T. (2013). Septin functions in organ system physiology and pathology. *Biol. Chem.* **395**, 123-141.

Finnigan, G. C., Takagi, J., Cho, C. and Thorner, J. (2015). Comprehensive Genetic Analysis of Paralogous Terminal Septin Subunits Shs1 and Cdc11 in *Saccharomyces cerevisiae*. *Genetics* **200**, 821-841.

Fuchs, U., Manns, I. and Steinberg, G. (2005). Microtubules are dispensable for the initial pathogenic development but required for long-distance hyphal growth in the corn smut fungus *Ustilago maydis*. *Mol. Biol. Cell* **16**, 2746-2758.

Fung, K. Y. Y., Dai, L. and Trimble, W. S. (2014). Cell and molecular biology of septins. *Int. Rev. Cell. Mol. Biol.* **310**, 289-339.

Garcia, G., III, Bertin, A., Li, Z., Song, Y., McMurray, M. A., Thorner, J. and Nogales, E. (2011). Subunit-dependent modulation of septin assembly: budding yeast septin Shs1 promotes ring and gauze formation. *J. Cell Biol.* **195**, 993-1004.

Garcia, G., III, Finnigan, G. C., Heasley, L. R., Sterling, S. M., Aggarwal, A., Pearson, C. G., Nogales, E., McMurray, M. A. and Thorner, J. (2016). Assembly, molecular organization, and membrane-binding properties of development-specific septins. *J. Cell Biol.* **212**, 515-529.

Haag, C., Steuten, B. and Feldbrügge, M. (2015). Membrane-coupled mRNA trafficking in fungi. *Annu. Rev. Microbiol.* **69**, 265-281.

Heasley, L. R. and McMurray, M. A. (2016). Roles of septins in prospore membrane morphogenesis and spore wall assembly in *Saccharomyces cerevisiae*. *Mol. Biol. Cell* **27**, 442-450.

Hernandez-Rodriguez, Y., Hastings, S. and Momany, M. (2012). The septin AspB in *Aspergillus nidulans* forms bars and filaments and plays roles in growth emergence and conidiation. *Eukaryot. Cell* **11**, 311-323.
Higuchi, Y., Ashwin, P., Roger, Y. and Steinberg, G. (2014). Early endosome motility spatially organizes polysome distribution. *J. Cell Biol.* **204**, 343-357.
Jansen, R.-P., Niessing, D., Baumann, S. and Feldbrügge, M. (2014). mRNA transport meets membrane traffic. *Trends Genet.* **30**, 408-417.
Kaplan, C., Jing, B., Winterflood, C. M., Bridges, A. A., Occhipinti, P., Schmied, J., Grinhagens, S., Gronemeyer, T., Tinnefeld, P., Gladfelter, A. S. et al. (2015). Absolute arrangement of subunits in cytoskeletal septin filaments in cells measured by fluorescence microscopy. *Nano Lett.* **15**, 3859-3864.
Kaufmann, A. and Philippsen, P. (2009). Of bars and rings: Hof1-dependent cytokinesis in multiseptated hyphae of *Ashbya gossypii*. *Mol. Cell. Biol.* **29**, 771-783.
Khan, A., McQuilken, M. and Gladfelter, A. S. (2015). Septins and generation of asymmetries in fungal cells. *Annu. Rev. Microbiol.* **69**, 487-503.
Koepke, J., Kaffarnik, F., Haag, C., Zarnack, K., Luscombe, N. M., König, J., Ule, J., Kellner, R., Begerow, D. and Feldbrügge, M. (2011). The RNA-binding protein Rrm4 is essential for efficient secretion of endochitinase Cts1. *Mol. Cell. Proteom.* **10**, M111.011213.
König, J., Baumann, S., Koepke, J., Pohlmann, T., Zarnack, K. and Feldbrügge, M. (2009). The fungal RNA-binding protein Rrm4 mediates long-distance transport of *ubi1* and *rho3* mRNAs. *EMBO J.* **28**, 1855-1866.
Kozubowski, L. and Heitman, J. (2010). Septins enforce morphogenetic events during sexual reproduction and contribute to virulence of *Cryptococcus neoformans*. *Mol. Microbiol.* **75**, 658-675.
Langner, T., Öztürk, M., Hartmann, S., Cord-Landwehr, S., Moerschbacher, B., Walton, J. D. and Göhre, V. (2015). Chitinases are essential for cell separation in *Ustilago maydis*. *Eukaryot. Cell* **14**, 846-857.
Lenz, J. H., Schuchardt, I., Straube, A. and Steinberg, G. (2006). A dynein loading zone for retrograde endosome motility at microtubule plus-ends. *EMBO J.* **25**, 2275-2286.
Loubradou, G., Brachmann, A., Feldbrügge, M. and Kahmann, R. (2001). A homologue of the transcriptional repressor Ssn6p antagonizes cAMP signalling in *Ustilago maydis*. *Mol. Microbiol.* **40**, 719-730.
McMurray, M. A., Bertin, A., Garcia, G., III, Lam, L., Nogales, E. and Thorner, J. (2011). Septin filament formation is essential in budding yeast. *Dev. Cell* **20**, 540-549.
Mostowy, S. and Cossart, P. (2012). Septins: the fourth component of the cytoskeleton. *Nat. Rev. Mol. Cell Biol.* **13**, 183-194.
Palacios, I. M. (2014). Hop-on hop-off: polysomes take a tour of the cell on endosomes. *J. Cell Biol.* **204**, 287-289.
Pohlmann, T., Baumann, S., Haag, C., Albrecht, M. and Feldbrügge, M. (2015). A FYVE zinc finger domain protein specifically links mRNA transport to endosome trafficking. *Elife* **4**, e06041.
Saarikangas, J. and Barral, Y. (2011). The emerging functions of septins in metazoans. *EMBO Rep.* **12**, 1118-1126.
Sadian, Y., Gatsogiannis, C., Patasi, C., Hofnagel, O., Goody, R. S., Farkasovsky, M. and Raunser, S. (2013). The role of Cdc42 and Gic1 in the regulation of septin filament formation and dissociation. *Elife* **2**, e01085.
Schuster, M., Kilaru, S., Fink, G., Collemare, J., Roger, Y. and Steinberg, G. (2011). Kinesin-3 and dynein cooperate in long-range retrograde endosome motility along a non-uniform microtubule array. *Mol. Biol. Cell.* **22**, 3645-3657.
Shaner, N. C., Campbell, R. E., Steinbach, P. A., Giepmans, B. N. G., Palmer, A. E. and Tsien, R. Y. (2004). Improved monomeric red, orange and yellow fluorescent proteins derived from *Discosoma* sp. red fluorescent protein. *Nat. Biotechnol.* **22**, 1567-1572.
Sirajuddin, M., Farkasovsky, M., Hauer, F., Kuhlmann, D., Macara, I. G., Weyand, M., Stark, H. and Wittinghofer, A. (2007). Structural insight into filament formation by mammalian septins. *Nature* **449**, 311-315.
Spiliotis, E. T. and Gladfelter, A. S. (2012). Spatial guidance of cell asymmetry: septin GTPases show the way. *Traffic* **13**, 195-203.
Spiliotis, E. T., Hunt, S. J., Hu, Q., Kinoshita, M. and Nelson, W. J. (2008). Epithelial polarity requires septin coupling of vesicle transport to polyglutamylated microtubules. *J. Cell Biol.* **180**, 295-303.
Stahl, Y., Grabowski, S., Bleckmann, A., Kuhnemuth, R., Weidtkamp-Peters, S., Pinto, K. G., Kirschner, G. K., Schmid, J. B., Wink, R. H., Hulsewede, A. et al. (2013). Moderation of Arabidopsis root stemness by CLAVATA1 and ARABIDOPSIS CRINKLY4 receptor kinase complexes. *Curr. Biol.* **23**, 362-371.
Steinberg, G. (2014). Endocytosis and early endosome motility in filamentous fungi. *Curr. Opin. Microbiol.* **20**, 10-18.
Stock, J., Sarkari, P., Kreibich, S., Brefort, T., Feldbrügge, M. and Schipper, K. (2012). Applying unconventional secretion of the endochitinase Cts1 to export heterologous proteins in *Ustilago maydis*. *J. Biotechnol.* **161**, 80-91.
Tada, T., Simonetta, A., Batterton, M., Kinoshita, M., Edbauer, D. and Sheng, M. (2007). Role of Septin cytoskeleton in spine morphogenesis and dendrite development in neurons. *Curr. Biol.* **17**, 1752-1758.
Tanaka-Takiguchi, Y., Kinoshita, M. and Takiguchi, K. (2009). Septin-mediated uniform bracing of phospholipid membranes. *Curr. Biol.* **19**, 140-145.
Versele, M., Gullbrand, B., Shulewitz, M. J., Cid, V. J., Bahmanyar, S., Chen, R. E., Barth, P., Alber, T. and Thorner, J. (2004). Protein-protein interactions governing septin heteropentamer assembly and septin filament organization in *Saccharomyces cerevisiae*. *Mol. Biol. Cell* **15**, 4568-4583.
Vida, T. A. and Emr, S. D. (1995). A new vital stain for visualizing vacuolar membrane dynamics and endocytosis in yeast. *J. Cell. Biol.* **128**, 779-792.
Vollmeister, E. and Feldbrügge, M. (2010). Posttranscriptional control of growth and development in *Ustilago maydis*. *Curr. Opin. Microbiol.* **13**, 693-699.
Vollmeister, E., Schipper, K., Baumann, S., Haag, C., Pohlmann, T., Stock, J. and Feldbrügge, M. (2012). Fungal development of the plant pathogen *Ustilago maydis*. *FEMS Microbiol. Rev.* **36**, 59-77.
Warenda, A. J., Kauffman, S., Sherrill, T. P., Becker, J. M. and Konopka, J. B. (2003). *Candida albicans* septin mutants are defective for invasive growth and virulence. *Infect. Immun.* **71**, 4045-4051.
Weidtkamp-Peters, S., Felekyan, S., Bleckmann, A., Simon, R., Becker, W., Kühnemuth, R. and Seidel, C. A. M. (2009). Multiparameter fluorescence image spectroscopy to study molecular interactions. *Photochem. Photobiol. Sci.* **8**, 470-480.
Xie, Y., Vessey, J. P., Konecna, A., Dahm, R., Macchi, P. and Kiebler, M. A. (2007). The GTP-binding protein Septin 7 is critical for dendrite branching and dendritic-spine morphology. *Curr. Biol.* **17**, 1746-1751.
Zhang, J., Kong, C., Xie, H., McPherson, P. S., Grinstein, S. and Trimble, W. S. (1999). Phosphatidylinositol polyphosphate binding to the mammalian septin H5 is modulated by GTP. *Curr. Biol.* **9**, 1458-1467.